



Tea polyphenols mediated Zero-valent Iron/Reduced graphene oxide nanocomposites for electrochemical determination of Hg^{2+}



Qian-Xin Bao^{a,b}, Yao Liu^{a,c}, Yue-Qing Liang^{a,c}, Rohan Weerasooriya^{a,d}, Heng Li^a, Yu-Cheng Wu^{a,b}, Xing Chen^{a,b,c,*}

^a Key Lab of Aerospace Structural Parts Forming Technology and Equipment of Anhui Province, Institute of Industry and Equipment Technology, Hefei University of Technology, Hefei 230009, PR China

^b School of Materials Science and Engineering, Hefei University of Technology, Hefei 230009, PR China

^c School of Resources and Environmental Engineering, Hefei University of Technology, Hefei 230009, PR China

^d National Centre for Water Quality Research, National Institute of Fundamental Studies, Kandy, Sri Lanka

ARTICLE INFO

Keywords:

Reduced graphene oxide
Tea polyphenols
Nano zero-valent iron
Electrochemical Determination
Mercury ions

ABSTRACT

Herein, we have developed a chemically modified glassy carbon electrode (GCE) using tea polyphenols mediated zero-valent iron/reduced graphene oxide nanocomposites (rGO-ZVI-P) for rapid determination of Hg^{2+} in water. Highly conductive rGO-ZVI-P were fabricated by a green chemical method using tea polyphenols as the reductant. The rGO-ZVI-P shows a unique affinity to aqueous Hg^{2+} due to a synergy between ZVI and rGO. The rGO-ZVI-P electrochemical sensor shows optimal performance for Hg^{2+} determination in pH 5.00 phosphate buffer and 180 s accumulation time at -1.2 V accumulation potential used under square wave anodic stripping voltammetry (SWASV). At these conditions, the Hg^{2+} determination sensitivity is $41.42 \mu\text{A}/\mu\text{M}$ and the determination limit is 1.2 nM. There are no interferences to the rGO-ZVI-P modified GCE sensor in the presence of $0.5 \mu\text{M}$ Cd^{2+} , $0.5 \mu\text{M}$ Pb^{2+} , and $0.5 \mu\text{M}$ Cu^{2+} in solution, either in discrete cations or multi-cations modes. Moreover, the typical chemical species found in the matrix of river water samples do not interfere with the as-fabricated Hg^{2+} electrochemical sensor. The Hg^{2+} determination by the rGO-ZVI-P modified GCE sensor is repeatable, stable, and robust, and it has potential in environmental applications.

1. Introduction

Mercury typically occurs as Hg^0 , Hg^{2+} , and methylated Hg in the environment. The toxicity of mercury species ordered as methylated $\text{Hg} > \text{Hg}^0 > \text{Hg}^{2+}$ causes serious damage to biota even in presence of minute concentrations of mercury species[1]. Mercury ions in the environment can enter the body through the food chain and combine with sulfhydryl groups in enzymes and proteins in the body to cause serious damage to the kidney and nervous systems. The US Environmental Protection Agency (EPA) requires that the content of mercury ions in drinking water should be less than 10 nM[2,3]. The major sources of mercury in the environmental systems include coal mining, fossil fuel burning, and various industrial activities[4,5]. In the environment, the formation of Hg^0 or methylated Hg seems to mediate via Hg^{2+} [6]. Therefore, developing a rapid and low-cost method for Hg^{2+} traces determination in water is timely.

Widely used mercury determination methods include high-performance liquid chromatography[7], colorimetry[8], inductively coupled plasma spectroscopy, atomic absorption spectrometry[9], etc. Although these methods are stable and accurate, most of them require costly equipment and complex operation procedures, so they are not suitable for in situ mercury analysis of environmental samples. Further, all of these methods determine total concentrations of mercury. On the contrary, the electrochemical methods have attracted attention because of their portability, simple operation, low cost, high efficiency, sensitivity, etc. They are also capable of determining chemical species[10]. Square wave anodic stripping voltammetry[11] (SWASV) is widely used as one of the most effective electrochemical methods for determining heavy metal ions. It is well known that electrochemical performance mainly depends on the electrode modification. At present, a large number of researchers are still devoted to the investigation of sensing materials, intending to construct the electrochemical interfaces with high activity, selectivity, and stability[12].

* Corresponding author.

E-mail address: xingchen@hfut.edu.cn (X. Chen).

Table 1
The electrochemical response of rGO-ZVI-P to Hg^{2+} compared with other reported materials.

Electrodes	Technique in details	Linear range (μM)	Sensitivity ($\mu\text{A}/\mu\text{M}$)	LOD (nM)	Correlation coefficient	Reference
MoS_2/rGO	SWASV	0.40–2.00	9.76	90.00	0.998	[43]
$[\text{Ru}(\text{bpy})_3]^{2+}/\text{GO}^{\text{a}}$	DPASV ^b	0.10–1.20	3.71	350.20	0.950	[44]
Graphene- MnO_2	LSV ^c	12.00–210.00	0.11	2000.00	0.993	[45]
N-doped graphene	DPSV ^d	0.07–9.00	15.73	10.00	0.987	[8]
SN-rGO ^e	SWASV	0.60–1.70	20.48	8.93	0.999	[47]
rGO-ZVI-P	SWASV	0.05–0.60	41.42	1.20	0.999	This work

^a ruthenium(II)-textured graphene oxide nanocomposite.

^b Differential pulse anodic stripping voltammetry.

^c Linear sweep voltammetry.

^d Differential pulse stripping voltammetry.

^e Assembling reduced graphene oxide with sulfur/nitrogen.

Nano zero-valent iron (ZVI) is environmentally benign and low cost. It can be used for pollution remediation[13] and pollutants determination[14]. Due to its high electrochemical activity and strong reduction ability, nano ZVI presents an enhanced electrochemical signal when used to construct an electrochemical sensing interface, and its electrochemical behavior is mainly manifested as improving the adsorption and electron transferring process[15,16]. When the heavy metal ions are adsorbed on the surface of the nano ZVI modified electrode, nano ZVI works as an electron donor that can promote the reduction of heavy metal ions, resulting in the highly sensitive determination of heavy metal ions[16,17]. However, nano ZVI is easy to aggregate and undergoes rapid oxidation upon exposure to the atmosphere, thus inhibiting its applications[18]. Halpegama et al.[19] used tea polyphenols as a reducing agent in the preparation with promising results, which minimized nano-zero valent iron aggregation and oxidation. Compared to chemical methods, the nano ZVI synthesized by tea polyphenols shows good dispersibility and stability in the atmosphere. The polyphenol route for nano zero-valent production is superior to conventional chemical synthesis [20]. Pu et al. [21] also noted that the preparation of zero-valent iron nanoparticles on the graphene framework is efficient in solving problems related to aggregation and oxidation.

Graphene, a two-dimensional honeycomb lattice material with a single atom thickness, has attracted attention due to its unique electronic, optical, chemical, mechanical, and thermal properties. To improve the application potential of graphene, researchers have carried out many modifications to the substrate [22]. Especially when combined with iron nanoparticles, e.g., zero-valent iron/reduced graphene oxide nanocomposites (rGO-ZVI) show an excellent adsorption effect for heavy metal ions. Ren and others[23] used chemically synthesized zero-valent iron/reduced graphene oxide to treat CrO_4^{2-} with promising results. The rGO skeleton prevents the accumulation of nano zero-valent iron particulates. The rGO-ZVI converts $\text{CrO}_4^{2-} \rightarrow \text{Cr}^{3+}$, which readily adsorb at negatively charged rGO. Wang et al. [24] also assembled nano zero-valent iron into graphene to remove arsenic and vanadium by adsorption. However, the determination of heavy metal ions using rGO-ZVI as a starting material for sensors has not been reported so far.

We have prepared rGO-ZVI-P by reducing Fe^{2+} on the rGO framework using tea polyphenols, which acts as a reductant and blocker during the synthesis process. The rGO-ZVI-P thus prepared was used to chemically modify glassy carbon electrode for electrochemical determination of Hg^{2+} by SWASV in water. The electrochemical behavior of the rGO-ZVI-P modified GCE was carefully optimized to maximize the sensitivity and robustness of Hg^{2+} determination. The determination mechanism of Hg^{2+} on the electrochemical sensing interface was also investigated. The chemical interference by divalent cations ubiquitous in aquatic systems, e.g., Cd^{2+} , Pb^{2+} , and Cu^{2+} on Hg^{2+} determination, was also examined. Finally, the new sensor's potential for

environmental applications was assessed by examining Hg^{2+} in a river water sample.

2. Experimental section

2.1. Materials and reagents

Tea polyphenols were purchased from Shanghai Macklin Biochemical Co., Ltd. All other analytical grade chemicals (e.g., graphite powder, H_2SO_4 (98%), NaNO_3 , KMnO_4 , HCl (37%), H_2O_2 (30%), $\text{FeSO}_4 \cdot 7\text{H}_2\text{O}$, etc.) were obtained from Sinopharm Chemical Reagent Co., Ltd (PR China) and used as received. 0.1 M acetic acid buffer (ABS) was prepared by mixing 0.1 M acetic acid with sodium acetate solution. 0.1 M phosphoric acid buffer (PBS) was prepared by mixing 0.1 M disodium hydrogen phosphate and potassium dihydrogen phosphate solution. 0.1 M citrate buffer (CPBS) was prepared from a mixture of 0.1 M citric acid and sodium citrate solution. Deionized water was used to prepare all solutions.

2.2. Preparation of zero-valent iron/reduced graphene oxide

2.2.1. Preparation of tea polyphenols mediated zero-valent iron/reduced graphene oxide (rGO-ZVI-P)

Graphene oxide (GO) was prepared according to the improved Hummers method. To synthesize rGO, tea polyphenols were added to a 10 g/L GO aqueous suspension while stirring for 30 min., continuously. The mixture color change from brownish yellow to black confirms the rGO formation. The rGO residue was washed with deionized water several times to a neutral pH and dried in a vacuum drying oven. To synthesize rGO-ZVI-P, rGO powder was dispersed in deionized water under sonication for 30 min to prepare 5 g/L rGO suspension, and then 0.25 M $\text{FeSO}_4 \cdot 7\text{H}_2\text{O}$ was added to 100 mL rGO suspension while shaking vigorously for 1 h. Afterward, 5 g/L tea polyphenols were added to rGO/ Fe^{2+} suspension, and stirring continued for 24 h to yield black colored rGO-ZVI-P. The rGO-ZVI-P was washed thoroughly with deionized water, dried, and stored in a vacuum drying oven.

2.2.2. Preparation of potassium borohydride reduced zero-valent iron/rGO (rGO-ZVI-B).

0.25 M ferrous sulfate was dissolved in 100 mL 5 g/L rGO solution and shaken vigorously for 1 h. Then, 25 mL of 1 M potassium borohydride solution was added to rGO/ $\text{FeSO}_4 \cdot 7\text{H}_2\text{O}$ suspension and stirred for 24 h. The resulting black material was washed to neutral and vacuum dried to obtain potassium borohydride reduced zero-valent iron/rGO (rGO-ZVI-B).

2.3. Characterization of rGO-ZVI-P

Field emission scanning electron microscopy (FE-SEM, Hitachi SU8020) and transmission electron microscopy (TEM, JEM-1400flash) were used to analyze the surface morphology, microstructure, and elemental composition of the rGO-ZVI-P. Raman spectra of the composites were obtained using a confocal laser Raman spectrometer (Raman, LabRAM HR Evolution HORIBA JOBIN YVON, Japan) at 532 nm. Near-surface elemental composition and functional groups of the materials were examined by X-ray photoelectron spectroscopy (ESCALAB250Xi Thermo, USA) and Fourier transform infrared spectroscopy (Thermo Nicolet, USA). N_2 adsorption and desorption were carried out by gas adsorption apparatus (BET, autosorb-IQ3, USA) at $-196\text{ }^\circ\text{C}$ to determine the specific surface area and pore size distribution.

2.4. Fabrication of rGO-ZVI-P modified glassy carbon electrode

The glassy carbon electrode (GCE) surface was chemically modified using rGO-ZVI-P, as given below. First, the electrode surface was polished with 1.0 μm , 0.3 μm , and 0.05 μm alumina powder to achieve a mirror surface. To remove residual alumina and other impurities from the surface, the GCE was then treated with 1:1 (v/v) HNO_3 , ethanol, and deionized H_2O successively by a continuous ultrasonic treatment for 2 min. 1 mg/mL rGO-ZVI-P suspension was prepared using dimethylformamide as a solvent. After intermittent shaking, the rGO-ZVI-P suspension was ultrasonicated for 30 min. A 6 μL rGO-ZVI-P droplets were placed on the electrode surface and then air-dried. A three-electrode system consisting of rGO-ZVI-P /GCE working electrode, $\text{Ag}|\text{AgCl}$ reference electrode, and Pt counter electrode were used for all measurements by an electrochemical workstation (CHI 760E, Chenghua Instrument Co., Ltd., China).

2.5. Electrochemical measurements

Electrochemical impedance spectroscopy (EIS) and cyclic voltammograms (CV) were used to study the electrochemical properties of the rGO-ZVI-P /GCE interface. Square wave anodic stripping voltammetry (SWASV) was used to determine Hg^{2+} . Parameter setting of EIS characterization: AC amplitude 5 mV, frequency ranging from 1 Hz to 10^6 Hz, DC potential 180 mV. The related parameters of SWASV are set as follows: potential range from -0.1 V to 0.6 V , increasing potential step of 4 mV, amplitude of 25 mV, and frequency of 15 Hz.

3. Results and discussion

3.1. Morphologic and structural characterization of rGO-ZVI-P

The morphology, microstructure, and elemental composition of rGO-ZVI-P composites were characterized by scanning electron microscopy (SEM) and transmission electron microscopy (TEM). As shown in SEM (Fig. 1.a), rGO-ZVI-P shows folds and pores intrinsic for rGO [25]. Such structures provide a large specific surface area for the attachment of ZVI. As shown in Fig. 1. b, the rGO-ZVI-P contains 34.6 % (Fe), 40.7% (C), and 24.6% (O), which confirms successful adherence of ZVI on the electrode surface. The observed O and C concentrations were largely derived from tea polyphenols and rGO. As shown in Fig. 1(c), the spherical ZVI particulates are uniformly dispersed on the folded rGO matrix. The ZVI agglomeration is largely avoided leading to a good sealing property of rGO[19,26]. According to Fig. 1. d, the measured lattice spacing is around 0.2 nm, corresponding to the (1 1 0) plane of Body Centred Cube (BCC) metallic Fe [27]. In addition, the energy spectrum of transmission electron microscopy shows uniformly distributed Fe^0 particulates on the surface of rGO.

The degree of defect and disorder in the graphene, reduced graphene oxide, and rGO-ZVI-P structures can be identified by Raman spectroscopy. Peaks D and G[28], respectively, represent the degree of carbon sp^2 and sp^3 hybridization. The peaks intensity ratio ($I_D: I_G$) measures the hybridization of carbon atoms in sp^2 and sp^3 modes and represents the degree of defect and disorder in the crystal structure. As shown in Fig. 2.a, peaks D and G appear at 1350 cm^{-1} and 1603 cm^{-1} . The $I_D: I_G$ ratio of rGO increased, indicating that GO was reduced to rGO, and the sp^2 conductive structure of graphene was repaired under the action of green tea polyphenols[29]. Notably, the $I_D: I_G$ ratio of rGO-ZVI-P increased, confirming the successful synthesis of the nanocomposite, as the loading of zero-valent iron provided more defect sites on rGO[30]. The peak shapes of rGO and rGO-ZVI-P are similar, indicating that the iron nanoparticles are loaded on the carbon skeleton without perturbing the graphene structure[31].

Fig. 2.b shows the Fourier transformed infrared spectra of GO, rGO, and rGO-ZVI-P. For GO, the broad band at 3411 cm^{-1} is related to the O—H stretching vibrations[32], the band at 1729 cm^{-1} is due to the stretching of C=O in $-\text{COOH}$, the band at 1390 cm^{-1} is due to the stretching of C—C[19], and the stretching vibration of C=C appears at 1624 cm^{-1} [33]. The C—O(alkoxy) and C—O(epoxy) bands appear at 1065 cm^{-1} and 1221 cm^{-1} [34], respectively. In the infrared spectra of rGO or rGO-ZVI-P, the C=O peak gradually disappeared, indicating that a large number of oxygen-containing functional groups were removed from GO under the action of tea polyphenols[35]. The C—O(epoxy) peak was due to hydrogen-bonded $-\text{COOH}$ deformation and was significantly strengthened upon reducing GO and Fe^{2+} with tea polyphenols. Compared with the rGO spectrum, the C—O peak at 1205 cm^{-1} in the rGO-ZVI-P spectrum shifted right, which may be related to the combination of graphene and ZVI particles. The Fe-O peaks appear at 602 and 472 cm^{-1} , corresponding to Fe-O in Fe_3O_4 and Fe_2O_3 [36]. This is because part of ZVI particles is oxidized, forming the adventitious core-shell structure of ZVI[37]. The shell composition is mainly ferric oxide, which is consistent with XPS analysis. ZVI may have π - π interactions with the rGO framework.

To further analyze the chemical composition and Fe valence states of the rGO-ZVI-P composite, an X-ray photoelectron spectroscopy (XPS) study was conducted (Fig. 3.c). The XPS diagram of rGO (Fig. 3.a) was used as a control. In the case of rGO-ZVI-P, the same peaks of C1s(283 eV) and O1s(530 eV) appear in the energy spectrum as those of rGO, and a new peak corresponds to Fe2p appears at 711 eV [23].

The type of C1s high-resolution peak of rGO-ZVI-P (Fig. 3 (d)) is attributed to rGO (Fig. 3 b), such as C=O(288.1 eV), C—O (285.3 eV), C—C/C=C(284.6 eV) [38], but the peak intensity changes. In rGO, C—C/C=C peaks are derived from the sp^2 (conjugated graphene) and sp^3 (removing O-derived functional groups) hybridization [37]. The C=O and C—O peaks are related to oxygen-containing functional groups' abundance in the composites [37]. In rGO-ZVI-P, the C1s intensity of C=O and C—O peaks decreased significantly, while the intensity of C—C/C=C peaks increased because the tea polyphenols used for $\text{Fe}^{2+} \rightarrow \text{Fe}^0$ conversion also reduced the oxygen-containing functional groups in graphene.

As shown in Fig. 3.e, the peaks of Fe2p correspond to the concurrent occurrence of Fe^{3+} , Fe^{2+} , and Fe^0 in rGO-ZVI-P. Peaks at 710.9 eV and 725.1 eV belong to Fe^{2+} , and peaks at 712.5 eV and 733.4 eV belong to Fe^{3+} [39]. The peak at 707.3 eV is caused by Fe^0 , while the corresponding satellite peak occurs at 719.5 eV. The spectral data confirms the successful incorporation of well-preserved ZVI particles on the graphene surface[40,41]. As shown in Fig. 3.e, the peak intensity of Fe^0 is small compared to Fe^{2+} and Fe^{3+} intensities. The XPS mainly analyzed the elemental composition of materials near-surface and their valence state. In the preparation of the rGO-ZVI-P composite, part of ZVI on the material's surface is slightly oxidized by oxygen in the air, forming a dense iron oxide shell on the surface.

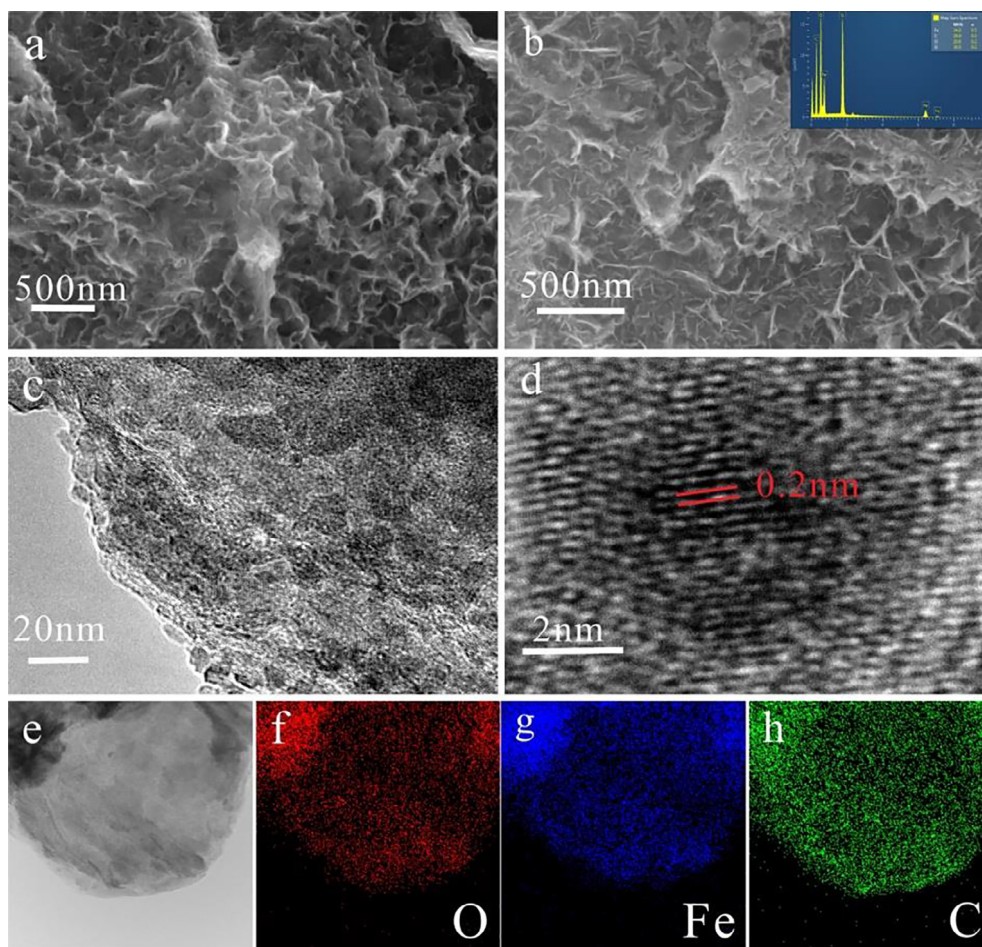


Fig. 1. SEM (a-b), TEM (c), HRTEM (d), and EDS mapping of oxygen (f), iron (g), and carbon (h) in the selected region (e) of rGO-ZVI-P nanomaterials, the inset in (b) is EDS analysis of rGO-ZVI-P.

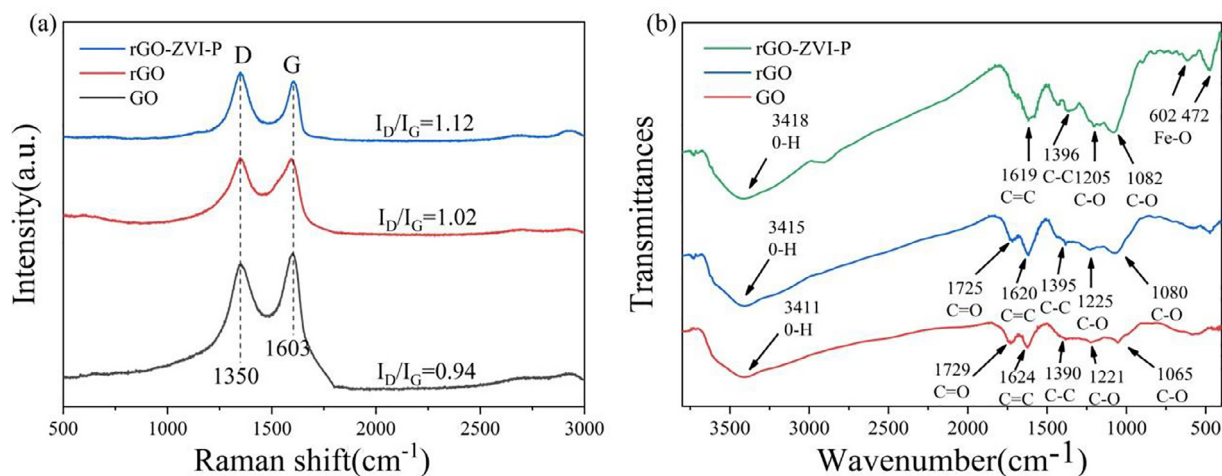


Fig. 2. Raman spectra (a) and Fourier transformed infrared spectra (b) of GO, rGO, and rGO-ZVI-P materials.

In the high-resolution figure of O1s (Fig. 3 (f)), a high strength Fe-O peak at 530.0 eV can be observed, but a large amount of ZVI is protected by tea polyphenols [42].

N_2 adsorption-desorption isotherms and pore size distribution of rGO and rGO-ZVI-P are shown in Fig. S1. The specific surface area of rGO after loading zero-valent iron decreases from 17.39 m^2/g to 12.37 m^2/g because zero-valent iron with a smaller diameter occupies the gap of rGO. The specific surface area of graphene decreases with

the loading of zero-valent iron. However, it still contains abundant micropores and mesopores, which is consistent with the previous data [24].

3.2. Electrochemical behavior of rGO-ZVI-P modified electrode

Cyclic voltammograms and electrochemical impedance spectroscopy were used to characterize the electrochemical properties

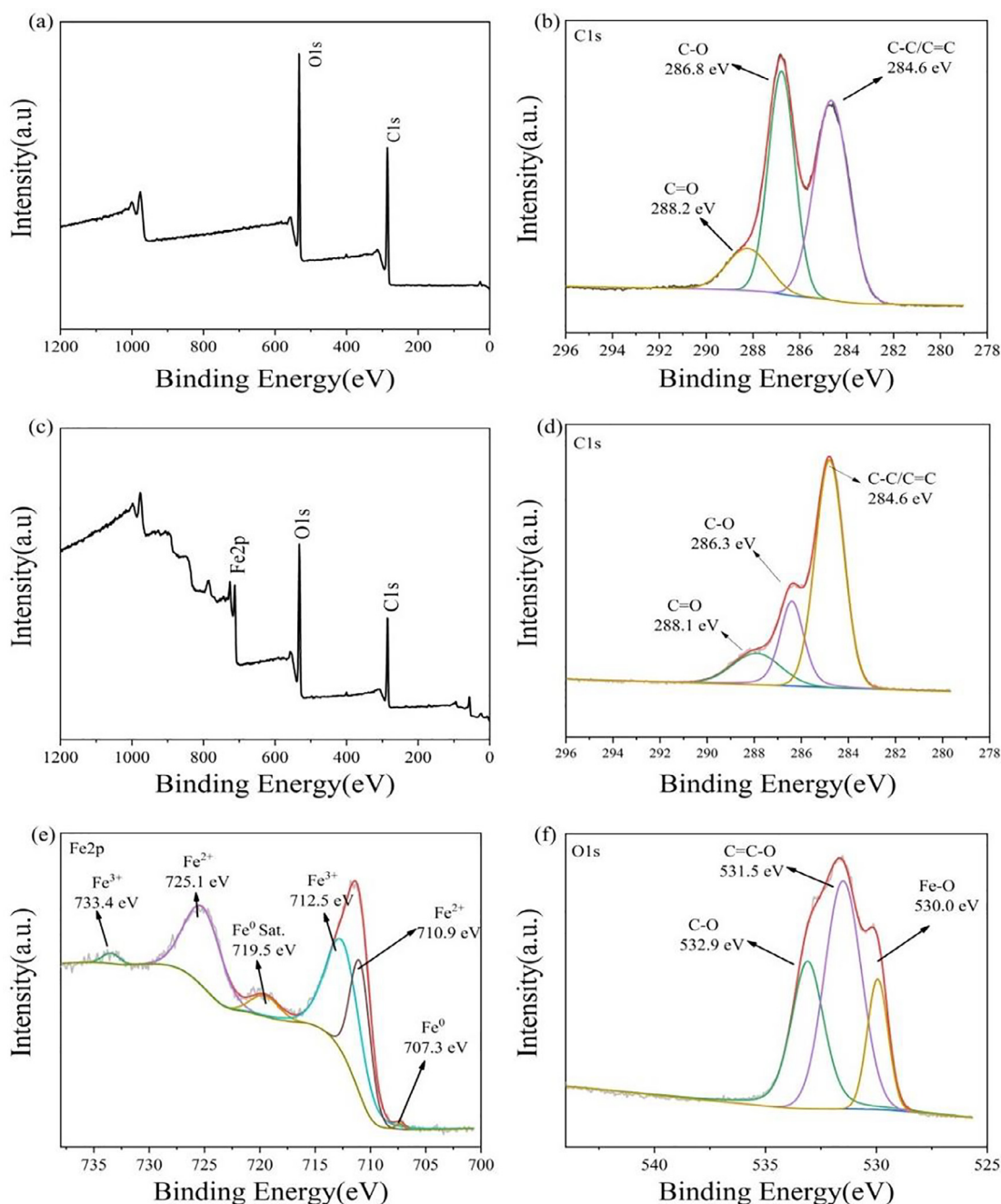


Fig. 3. XPS total spectrum of rGO (a), the high-resolution spectrum of C1s (b), XPS total spectrum of rGO-ZVI-P (c), the high-resolution spectrum of C1s (d), the high-resolution spectrum of Fe2p (e), and high-resolution spectrum of O1s (f).

and the electrons transfer kinetics at the solid–liquid interface of the rGO-ZVI-P modified GCE. The CV and EIS of bare GCE, rGO, and rGO-ZVI-P modified GCE were examined in 5 mM Fe (CN)₆^{3-/4-} in 0.1 M KCl. As shown in Fig. 4a, the three electrodes maintain a high and symmetrical redox peak. Among them, the potential difference of the bare GCE is the lowest, while the potential difference of the rGO-ZVI-P modified GCE increases, indicating that the composite material successfully modified the surface of the electrode. Compared to the CV curve of rGO modified GCE, the peak current of rGO-ZVI-P modified GCE is increased. The ZVI on rGO promotes more efficient electron transfer than rGO or bare GCE surface.

Fig. 4b shows a typical Nyquist diagram of the rGO-ZVI-P modified GCE in three electrodes configuration using EIS data. The magnitude

of the diameter of the semi-circle shows a measure of electron transfer resistance at high frequencies. In contrast, the linear part shows the diffusion limiting process at low frequencies. Through equivalent circuit simulation, the EIS data of the modified electrodes were analyzed (inset of Fig. 4. b), R₁ represents solution resistance, R₂ represents electron transfer resistance, W_o represents Warburg impedance, and CPE represents constant phase angle element. See Table S1 for the specific data of each circuit component. The EIS curve of rGO-ZVI-P modified GCE is consistent with the CV result. Compared to the bare GCE, the R₂ value of the rGO modified GCE and the rGO-ZVI-P modified GCE increased obviously, and the R₂ value of the rGO-ZVI-P modified GCE was lower than that of the rGO modified GCE. The rGO contains many oxygen-rich functional groups, which hinder the electron trans-

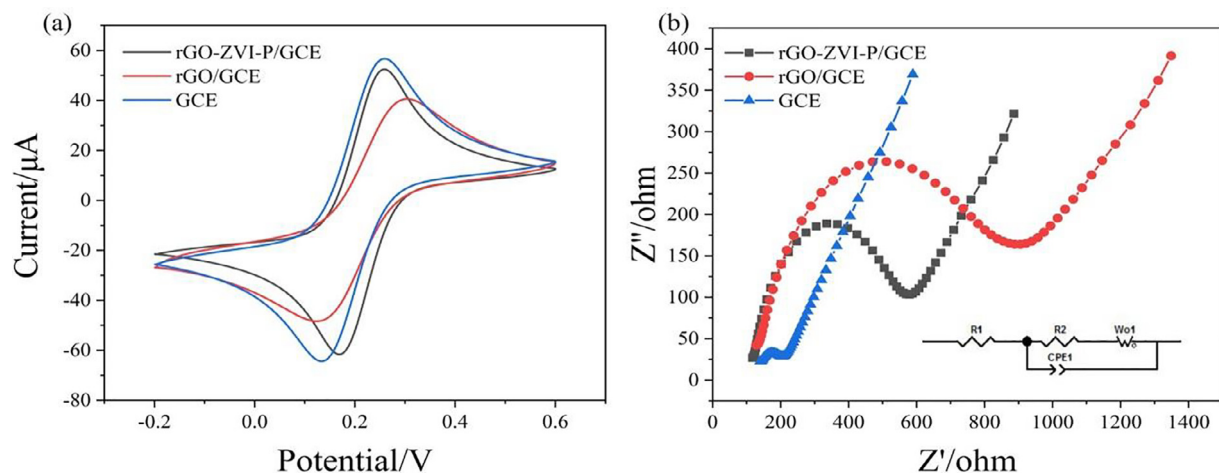


Fig. 4. Cyclic voltammograms (a) and typical Nyquist curves (b) of GCE, rGO /GCE, rGO-ZVI-P /GCE in a solution containing 5 mM $\text{Fe}(\text{CN})_6^{3-/4-}$ and 0.1 M KCl, the inset is an equivalent circuit model.

fer at the solid–liquid interface. However, with the introduction of ZVI into rGO, the electron transfer rate at the electrode and solution interface is enhanced.

3.3. Optimisation of experimental electrochemical conditions

rGO-ZVI-P modified GCE was used for electrochemical Hg^{2+} determination in environmental samples. The Hg^{2+} determination sensitivity by the rGO-GCE sensor can be improved in two ways; by improving electron transfer dynamics at the electrode-solution interface and by varying experimental parameters used in analyte determination. The experimental and instrument parameters optimized for Hg^{2+} determination are pH, buffer type, accumulation time, and accumulation potential. At a time, only one parameter was varied while keeping others fixed. In all cases, $0.5 \mu\text{M}$ Hg^{2+} was used.

For choosing a suitable buffer type, three buffers, namely 0.1 M acetate buffer (ABS), 0.1 M citrate buffer (CPBS), and 0.1 M phosphate buffer (PBS) were selected. In the solution containing $0.5 \mu\text{M}$ Hg^{2+} , at -1.2 V accumulation potential with 100 s accumulation time, the observed voltammograms are shown in Fig. 5 (a). The peak current for Hg^{2+} in PBS buffer is the highest. Therefore, 0.1 M phosphate buffer was selected for Hg^{2+} determination experiments out of three buffers examined.

To optimize the pH value, 0.1 M PBS solutions at pH values ranging from ~ 3.00 to ~ 6.00 were used. The accumulation time and accumulation potential were fixed at 100 s and -1.2 V, respectively. The voltammograms are shown in Fig. 5. b. When pH varied from ~ 3.00 to ~ 6.00 , the current shows an optimal value at pH 5.00. This may be due to the “crowding out” of mercury by hydrogen ions in solution at acidic pH, while hydrolysis occurs at basic pH. Therefore, the choice of pH ~ 5.00 PBS buffer is most appropriate for Hg^{2+} determination.

The accumulation potentials at the rGO-ZVI-P sensor were investigated between -1.0 and -1.5 V. The voltammograms are shown in Fig. 5. c. With the increase of the accumulation potential, the response current increased first and then decreased. The maximum current value is observed at -1.2 V. Further increase of potential favors Hg^{2+} reduction in solution, which increases oxidized ions in the second stage and a strong electrochemical signal at the electrode interface. However, at high potential, H^+ is also reduced to hydrogen gas that collects at the interface of the electrode forming gaseous bubbles, which hinders the Hg^{2+} reduction. So the optimal accumulation potential at -1.2 V was chosen for the subsequent investigation.

An additional experiment was carried out to determine the Hg^{2+} accumulation time on the rGO-ZVI-P modified electrode. The accumu-

lation time of Hg^{2+} accumulation varied between 90 s and 240 s. The voltammograms are given in Fig. 5d. With the increase of accumulation time, the number of Hg^{2+} on the surface of the working electrode increases, and the response current increases. Between the 90 s and ~ 180 s range, the current increases rapidly, and in the 180 s and ~ 240 s range, the response current only slightly increases. This may be because the mercury ions in the solution have reached the saturation state at the electrode interface when the accumulation time is 180 s. For subsequent experiments, we used the following optimized parameters; pH 5.00 0.1 M phosphate buffer, accumulation potential -1.20 V, and 180 s accumulation time.

3.4. Electrochemical determination of Hg^{2+} with rGO -ZVI modified GCE

The GCE modified by rGO or rGO-ZVI-P composites was used to develop an electrochemical sensor for Hg^{2+} determination by square wave anodic stripping voltammetry (SWASV). Bare GCE was used as a control. Compared to the control, the rGO modified GCE shows an enhanced signal for Hg^{2+} determination due to the abundance of active sites for analyte retention. Fig. 6 (a) shows the voltammograms of $0.5 \mu\text{M}$ Hg^{2+} measured with rGO and rGO-ZVI-P modified GCE in pH ~ 5.00 solution. Compared to the bare electrode surface, rGO modified surface provides a larger specific surface area (e.g., active sites), showing enhanced sensitivity for Hg^{2+} determination. ZVI is a catalyst for Hg^{2+} reduction. When ZVI adheres to the rGO skeleton, uniformly dispersed sites are generated on the surface (designated as rGO-ZVI-P). The electron transfer dynamics is facilitated via $\text{Fe}(\text{O})/\text{Fe}(\text{II})/\text{Fe}(\text{III})$ redox couples[14]. The removal of O-derived functional groups and repair of sp^2 structures enhanced the composites' electric conductivity, which signifies the increase of peak current for Hg^{2+} by about six times.

Under optimal conditions, the GCE modified with rGO-ZVI-P was used to determine Hg^{2+} in the solution, and the voltammograms are shown in Fig. 6 (b). The nearly parallel voltammograms showed a steep peak indicating the electrochemical signal for Hg^{2+} determination at 0.17 V. To examine the sensor's sensitivity, Hg^{2+} concentrations were incremented by $0.05 \mu\text{M}$ steps in each cycle. As the Hg^{2+} concentration increased, the peak current increased, and it is linear with the Hg^{2+} concentration ($Y(\mu\text{A}) = 41.42 X (\mu\text{M}) - 1.66$; $R^2 = 0.999$). The electrode's sensitivity is $41.42 \mu\text{A}/\mu\text{M}$, and the limit of detection (LOD) is 1.2 nM based on the $3\delta/S$ estimation method (S represents the slope of the linear fitting equation, and δ represents the signal-to-noise ratio(S/N)). Table 1 summarizes the sensitivity, LOD, and linear dynamic range of Hg^{2+} determination by different electro-

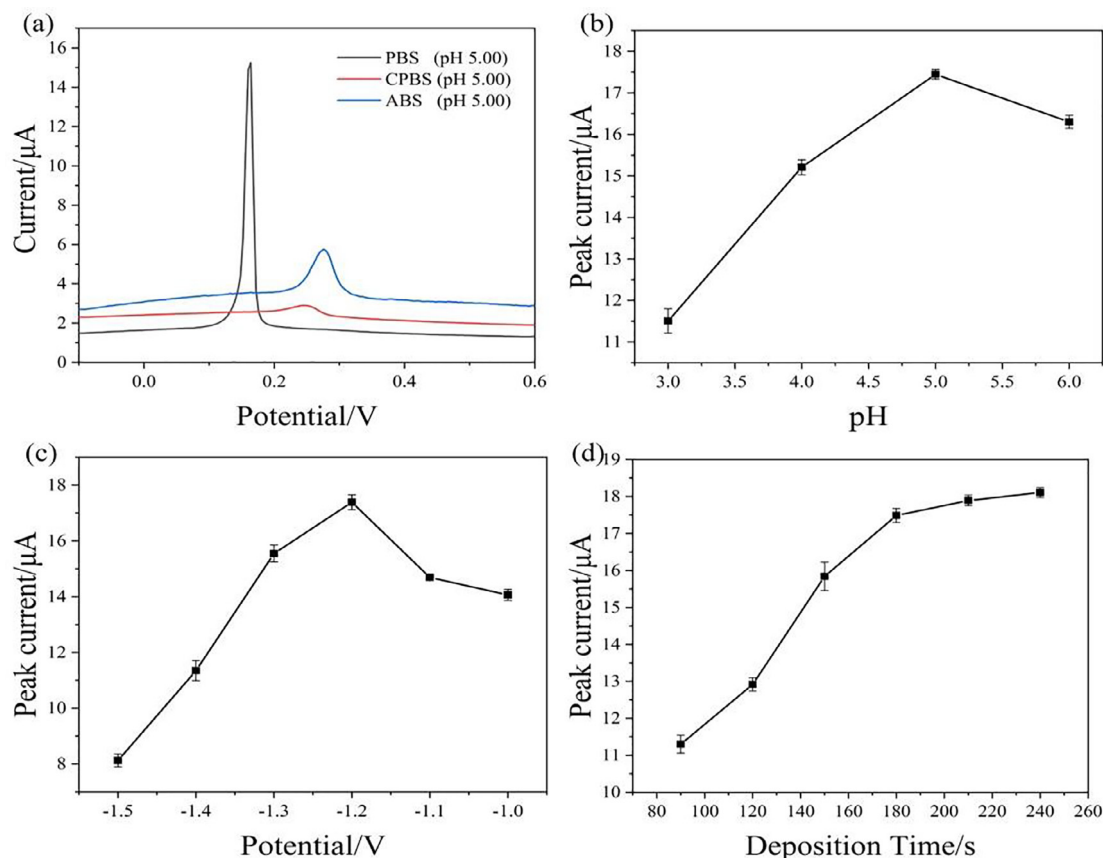


Fig. 5. Optimization experiment of rGO-ZVI-P modified electrode: (a) buffer type, (b) pH value of solution, (c) accumulation potential, (d) accumulation time.

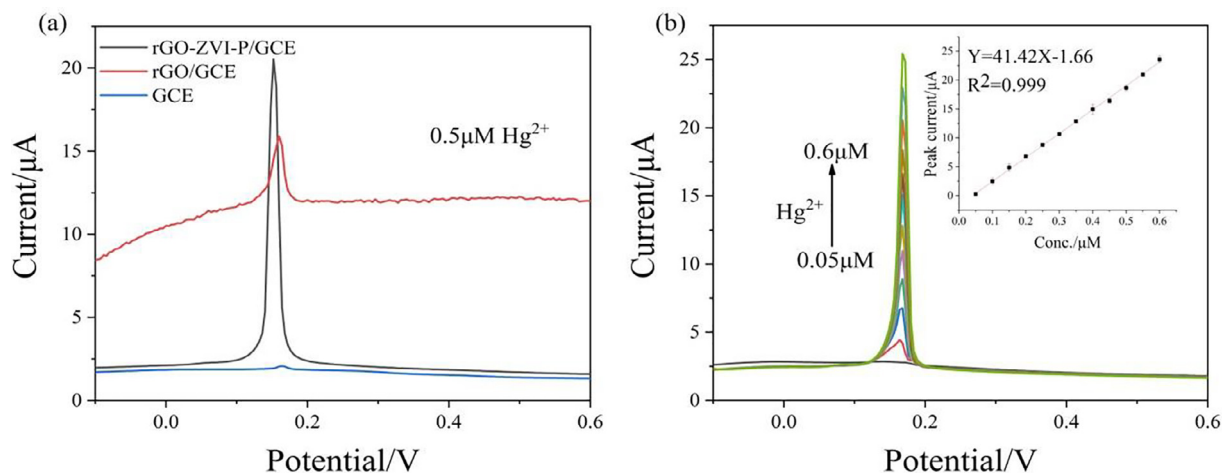


Fig. 6. Typical SWASV responses of 0.5 μM mercury ions on naked GCE, rGO and rGO-ZVI-P modified glassy carbon electrodes (a) and electrochemical response of rGO-ZVI-P to different concentrations of mercury ions under optimized conditions (b).

chemical methods using various sensors. Our results show the enhanced performance of the rGO-ZVI-P electrochemical sensor compared to others.

3.5. Possible mechanisms.

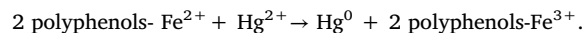
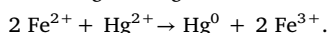
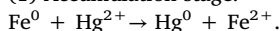
From the above results, it can be found that the rGO-ZVI-P was prepared by using tea polyphenols as reductants and protectors. The sp² structure of graphene improves the conductivity of ZVI, and rGO may interact with ZVI through π-π. In the follow-up electrochemical

test of Hg²⁺, it was found that the loading of highly active ZVI particles significantly enhanced the electrochemical response to mercury ions. However, the possible reaction mechanism between ZVI, tea polyphenols, and mercury ions is not clear. Therefore, we designed to prepare zero-valent iron nanoparticles (rGO-ZVI-B) on graphene framework using potassium borohydride as reductant, and analyze the electrochemical behavior of mercury ions under the same conditions. The results showed that (Fig. S2), the sensitivity and determination limit of the sensor were both lower than rGO-ZVI-P. The stripping peak current of rGO-ZVI-B/GCE was only 2/3 of that of rGO-ZVI-P/

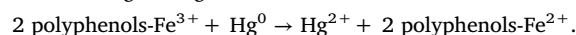
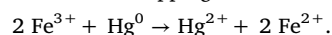
GCE at the same concentration of mercury ion, which may be related to the lack of ZVI active sites on graphene surfaces.

In the absence of a protective agent, the zero-valent iron attached to the graphene surface agglomerates and forms an iron oxide on contact with air, forming a dense iron oxide shell that blocks electron migration. In addition, the absence of zero-valent iron at metal sites weakens the $\text{Fe}^{2+}/\text{Fe}^{3+}$ cycle[16], resulting in a corresponding reduction in response current. Tea polyphenols not only play the role of a green reductant but also can be used as a blocker of ZVI to improve the dispersity (Fig. 1(c)) and stability of ZVI. In the presence of tea polyphenols, ZVI particles loaded on the surface of rGO can prevent further oxidation by oxygen. Tea polyphenols have no reduction ability to mercury ions, but tea polyphenols easy form a stable polyphenol- Fe^{2+} structure with Fe^{2+} [19], that is, the graphene surface contains a large number of ZVI particles, Fe^{2+} and polyphenols- Fe^{2+} structure, which is conducive to the reduction reaction of mercury ions in the accumulation stage. However, only a small amount of ZVI active sites and Fe^{2+} were found in rGO-ZVI-B material. After contact with air, the polyphenols- Fe^{2+} structure will slowly change to a polyphenols- Fe^{3+} structure[48], which shows that the reduction potential of Fe^{2+} decreases and the oxidation rate of ZVI increases. Combined with relevant literature [49], the possible mechanisms of ZVI, tea polyphenols, and Hg^{2+} can be roughly divided into mercury ion accumulation and oxidation:

(1) Accumulation stage.



(2) SWASV stripping.



3.6. Interference experiments with other metal ions

The interference of selected divalent cations on Hg^{2+} determination by rGO-ZVI-P modified GCE sensor was examined in two modes: (1) Discrete cations mode where only one foreign cation is added at a time; (2) Concurrent cations mode where all cations are added at once. At any time, the concentration of a foreign cation is $0.5 \mu\text{M}$, and the Hg^{2+} concentration was varied between 0.1 and $0.9 \mu\text{M}$. Irrespective of the presence of foreign cations, the Hg^{2+} peaks are sharp, and the variation of peak current intensity vs concentration of Hg^{2+} is always linear (Fig. 2S). In all cases, Hg^{2+} shows an anomalous affinity for rGO-ZVI-P over other cations present in the solution. However, the intensity of Cu^{2+} and Cd^{2+} peaks enhanced significantly due to the formation of $\text{Hg}(\text{O})$ thin film on the electrode surface facilitating Cd or Cu and mercury amalgamation[50,51]. However, the current peak of Pb^{2+} appeared only once and then disappeared forming $\text{Pb}_3(\text{PO}_4)_2$ precipitate with phosphate present excessively in the buffer solution. The Hg^{2+} determination sensitivity of the rGO-ZVI-P modified GCE has decreased in the presence of Cd^{2+} , Pb^{2+} , and Cu^{2+} . Of the three

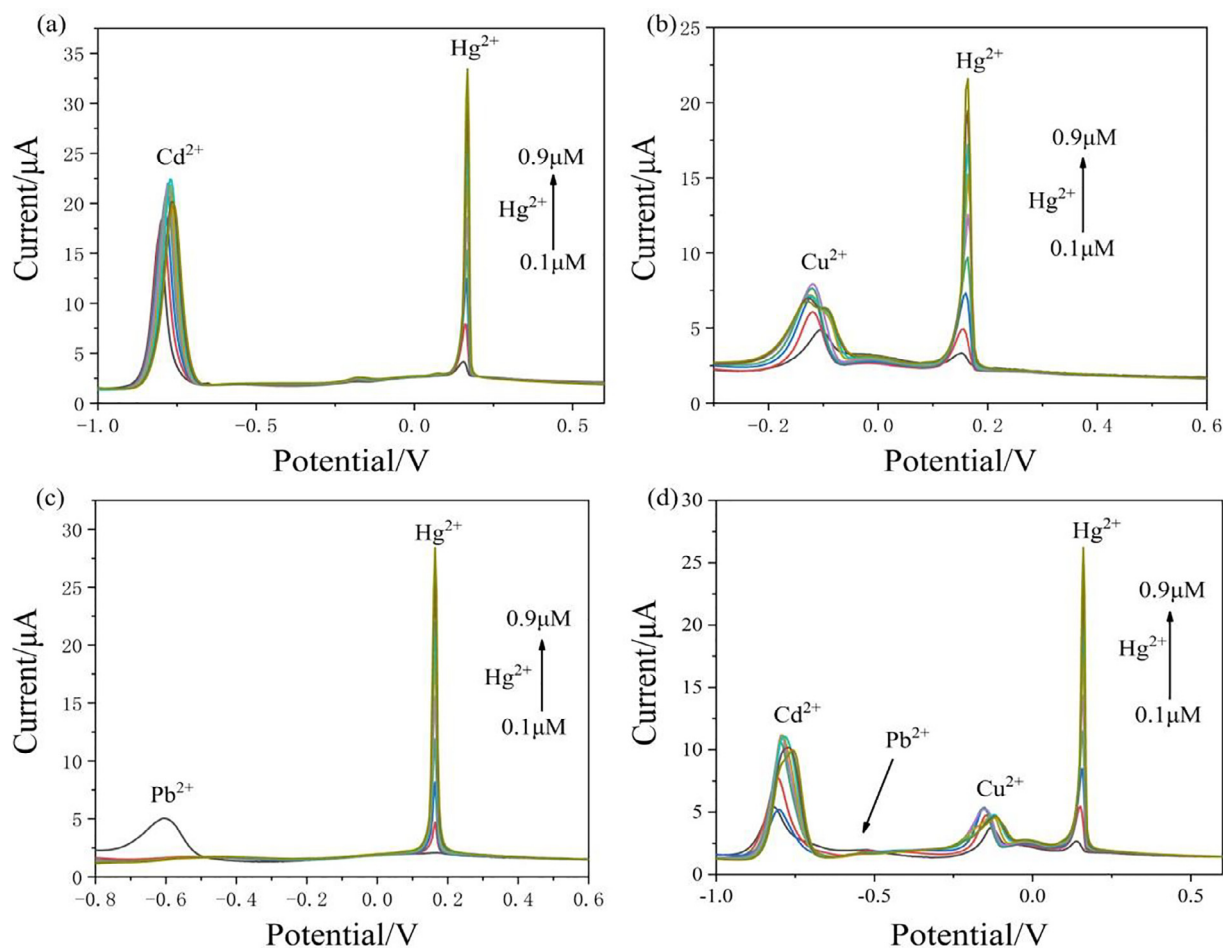


Fig. 7. SWASV responses of rGO-ZVI-P modified electrode to a series of concentrations of Hg^{2+} . (a) in the presence of $0.5 \mu\text{M}$ Cd^{2+} , (b) in the presence of $0.5 \mu\text{M}$ Cu^{2+} , (c) in the presence of $0.5 \mu\text{M}$ Pb^{2+} , (d) in the presence of $0.5 \mu\text{M}$ Cd^{2+} , Cu^{2+} , Pb^{2+} , etc.

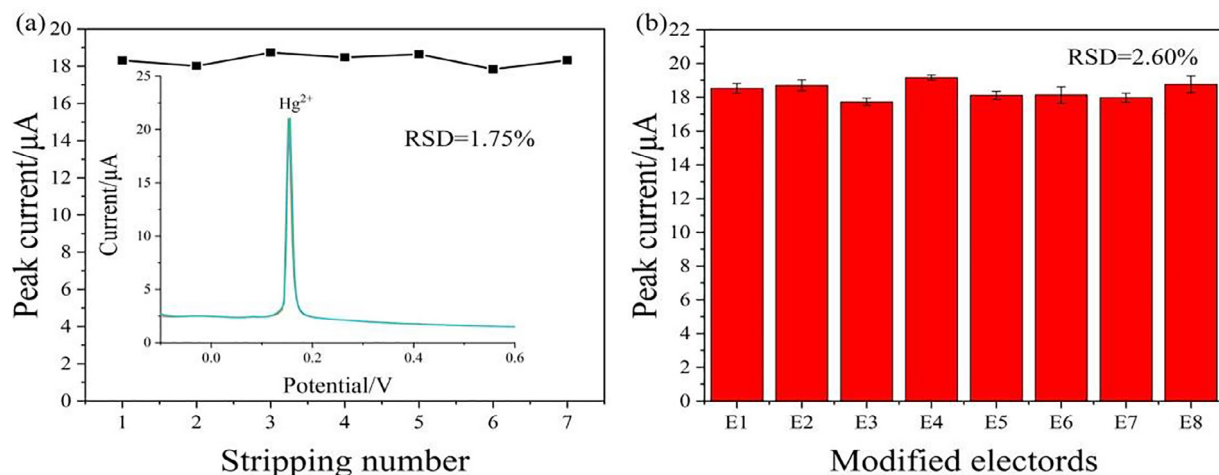


Fig. 8. Stability and reproducibility of rGO-ZVI-P/GCE. (a) The SWASV responses toward $0.5 \mu\text{M Hg}^{2+}$ on seven consecutive days. The inset is the typical voltammograms curve. (b) The SWASV responses toward $0.5 \mu\text{M Hg}^{2+}$ of 8 rGO-ZVI-P/GCEs.

cations examined, Cu^{2+} shows the maximum interfering effect for Hg^{2+} determination, and the sensitivity decreased to $23.40 \mu\text{A} \cdot \mu\text{M}^{-1}$.

Under the same experimental conditions, the Hg^{2+} determination was also examined under concurrent cations mode, and the voltammograms are given in Fig. 7. d. In this system, with the increase of Hg^{2+} concentration in a stepwise fashion, the corresponding current peaks of Cd^{2+} and Cu^{2+} increased slightly. The peak of Pb^{2+} disappeared completely, which can be ascribed to the arguments made earlier. However, the peak and sensitivity of cations decreased in the concurrent cations mode compared to the single cation mode. The sensitivity of Hg^{2+} determination under the concurrent mode has decreased to $29.83 \mu\text{A} \cdot \mu\text{M}^{-1}$. However, it is also observed that even in the presence of a single or multiple foreign cations, the current peak of Hg^{2+} is well separated from the other current peaks. Its peak current is much higher than that of foreign cations. Moreover, in the presence of interfering cations, the peak current and Hg^{2+} concentration still show an excellent linear relationship ($R^2 = 0.999$) which confirms the selectivity of rGO-ZVI-P sites for Hg^{2+} retention.

3.7. Stability and reproducibility

The precision and stability of measurement by rGO-ZVI-P modified GCE were examined using a $0.5 \mu\text{M Hg}^{2+}$ solution. The new electrochemical sensor was used repeatedly for a week. As shown in Fig. 8 (a), the current response peaks of the 7 experiments coincide. The relative standard deviation (RSD) of the measurements is 1.75 % which indicates the stability of the sensor for repeated use under robust conditions. In another experiment, we fabricated eight rGO-ZVI-P modified GCE sensors to assess reproducibility for Hg^{2+} determination. The response curve is shown in Fig. 8 (b). The current peak of eight sensors is consistent, and the RSD of the current peak is about 2.60% indicating that the electrode fabrication has good precision.

3.8. Determination of spiked Hg^{2+} in the natural river water

The rGO-ZVI-P modified GCE sensor was also used to check the feasibility and robustness of metal ions determination in real water analysis. We collected a natural water sample from Nanfeihe River (Hefei, PR China) for Hg^{2+} analysis using the rGO-ZVI-P modified GCE sensor developed by us. After storing the river water for 24 h, it was mixed with 0.1 M phosphate buffer at a 1:9 ratio (sample: buffer) to yield a solution with a pH value of ~ 5.00 . We noted that there was no Hg^{2+} contamination or the Hg^{2+} concentration in the river water was below the determination limit, viz., 1.2 nM. Multiple Hg^{2+} spike

analysis of river water was carried out to determine matrix effects of river water. The i vs C result from the voltammograms shows a linear relationship (Fig. S4). The matrix species in river water seemed to have negligible effect on Hg^{2+} determination. The Hg^{2+} recovery rates by spiked analysis are always around $100 \% \pm 3\%$ (Table S1 for details). Our data conclude that the matrix effects of river water on Hg^{2+} determination by the new electrochemical sensor could be negligible.

4. Conclusions

We fabricated an rGO-ZVI-P modified GCE sensor for trace determination of Hg^{2+} in water by square wave anode stripping voltammetry (SWASV) with $41.22 \mu\text{A}/\mu\text{M}$ sensitivity and 1.2 nM determination limit. Compared to bare GCE or rGO modified GCE sensors, the Hg^{2+} determination by rGO-ZVI-P modified GCE shows 3.45 ~ 2.17-fold higher sensitivity. The rGO-ZVI-P modified GCE showed minimal interference for Hg^{2+} determination by the presence of equimolar Cd^{2+} , Cu^{2+} , and Pb^{2+} in solution. The chemically modified GCE shows good precision and stability in the Hg^{2+} determination of natural waters. The rGO-ZVI-P is environmentally benign and robust, which offers an ideal sensor for in situ Hg^{2+} trace determination in environmental samples.

CRedit authorship contribution statement

Qian-Xin Bao: Methodology, Formal analysis, Investigation, Writing – original draft. **Yao Liu:** Methodology, Investigation, Formal analysis. **Yue-Qing Liang:** Formal analysis. **Rohan Weerasooriya:** Writing – review & editing. **Heng Li:** Formal analysis. **Yu-Cheng Wu:** Formal analysis, Resources. **Xing Chen:** Conceptualization, Supervision, Writing – review & editing, Funding acquisition.

Declaration of Competing Interest

The authors declare that they have no known competing financial interests or personal relationships that could have appeared to influence the work reported in this paper.

Acknowledgments

The authors acknowledge the financial support from the National Natural Science Foundation of China (Grant No. 21777164), and Key Science and Technology Projects of Anhui Province

(202003a07020004). R. W. acknowledges the Program of Distinguished Professor in B&R Countries (Grant No. G20200012010).

Appendix A. Supplementary data

Supplementary data to this article can be found online at <https://doi.org/10.1016/j.jelechem.2022.116428>.

References

- [1] M.C. Colin Bard, *Environmental Chemistry*, fifth ed., UKP, WH Freeman, 2012, p. 776.
- [2] P.B. Tchounwou et al, Environmental exposure to mercury and its toxicopathologic implications for public health, *Environ Toxicol* 18 (3) (2003) 149–175.
- [3] N. Jeromiyas, E. Elaiyappillai, A.S. Kumar, S.-T. Huang, V. Mani, Bismuth nanoparticles decorated graphenated carbon nanotubes modified screen-printed electrode for mercury detection, *Journal of the Taiwan Institute of Chemical Engineers* 95 (2019) 466–474.
- [4] H.R. Akbari Hasanani, K. Zarei, An electrochemical sensor for attomolar determination of mercury(II) using DNA/poly-L-methionine-gold nanoparticles/pencil graphite electrode, *Biosens Bioelectron* 128 (2019) 1–8.
- [5] M.M. Rahman, K.A. Alamry, M.R. Awual, A.E.M. Mekky, Efficient Hg(II) ionic probe development based on one-step synthesized diethyl thieno[2,3-b]thiophene-2,5-dicarboxylate (DETTDC2) onto glassy carbon electrode, *Microchemical Journal* 152 (2020) 104291.
- [6] G. Kaiser, G.T., *Mercury In: The Handbook of Environmental Chemistry* (ed. O. Hutzinger) Springer, Germany, 2013: p. 1-43.
- [7] L. Wang, J.-B. Zhou, X. Wang, Z.-H. Wang, R.-S. Zhao, Simultaneous determination of copper, cobalt, and mercury ions in water samples by solid-phase extraction using carbon nanotube sponges as adsorbent after chelating with sodium diethyldithiocarbamate prior to high performance liquid chromatography, *Anal Bioanal Chem* 408 (16) (2016) 4445–4453.
- [8] Y. Zhang, H. Chen, D. Chen, D.i. Wu, Z. Chen, J. Zhang, X. Chen, ShengHua Liu, J. Yin, A colorimetric and ratiometric fluorescent probe for mercury (II) in lysosome, *Sensors and Actuators B: Chemical* 224 (2016) 907–914.
- [9] F. Domanico, G. Forte, C. Majorani, O. Senofonte, F. Petrucci, V. Pezzi, A. Alimonti, Determination of mercury in hair: Comparison between gold amalgamation-atomic absorption spectrometry and mass spectrometry, *J Trace Elem Med Biol* 43 (2017) 3–8.
- [10] Q.i. Ding, C. Li, H. Wang, C. Xu, H. Kuang, Electrochemical detection of heavy metal ions in water, *Electrochemical detection of heavy metal ions in water*. 57 (59) (2021) 7215–7231.
- [11] D. Jadreško, M. Lovrić, A theory of square-wave voltammetry of surface-active, electroinactive compounds, *Electrochimica Acta* 53 (27) (2008) 8045–8050.
- [12] D. Dai, J. Yang, Y. Wang, Y.-W. Yang, Recent Progress in Functional Materials for Selective Detection and Removal of Mercury(II), *Ions*. *Advanced Functional Materials* 31 (1) (2021) 2006168.
- [13] G. Sharma, A. Kumar, S. Sharma, A.H. Al-Muhtaseb, M.u. Naushad, A.A. Ghfar, T. Ahamad, F.J. Stadler, Fabrication and characterization of novel FeO@Guar gum-crosslinked-soya lecithin nanocomposite hydrogel for photocatalytic degradation of methyl violet dye, *Separation and Purification Technology* 211 (2019) 895–908.
- [14] M. Yang et al, Zero-valent iron nanomaterial Fe(0)/Fe₂MnO₄ for ultrasensitive electroanalysis of As(III): Fe(0) influenced surficial redox potential, *Chem Commun (Camb)* 57 (11) (2021) 1324–1327.
- [15] Y. Zou, X. Wang, A. Khan, P. Wang, Y. Liu, A. Alsaedi, T. Hayat, X. Wang, Environmental remediation and application of nanoscale zero-valent iron and its composites for the removal of heavy metal ions: A review, *Environ Sci Technol* 50 (14) (2016) 7290–7304.
- [16] S.-H. Chen, J.-J. Zhu, P.-H. Li, Y.-F. Sun, M. Yang, X.-J. Huang, In-situ growth of zero-valent iron in FeO_x/Mn₃O₄ to improve the surficial redox for high-efficient electrocatalysis of Pb(II), *Chemical Engineering Journal* 430 (2022) 132959.
- [17] L. Ling, C. Tang, W.-X. Zhang, Visualization of silver nanoparticle formation on nanoscale zero-valent iron, *Environmental Science & Technology Letters* 5 (8) (2018) 520–525.
- [18] J. Guo, R. Wang, W.W. Tjii, J. Pan, T. Liu, Synthesis of Fe nanoparticles@graphene composites for environmental applications, *J Hazard Mater* 225-226 (2012) 63–73.
- [19] J.U. Halpegama, P.M.C.J. Bandara, L. Jayarathna, A. Bandara, C.-Y. Yeh, J.-Y. Chen, C. Kuss, U. Dahanayake, A.C. Herath, S.K. Weragoda, X. Chen, R. Weerasooriya, Facile fabrication of nano zerovalent iron – Reduced graphene oxide composites for nitrate reduction in water. *Environmental, Advances* 3 (2021) 100024.
- [20] T. Wang, J. Lin, Z. Chen, M. Megharaj, R. Naidu, Green synthesized iron nanoparticles by green tea and eucalyptus leaves extracts used for removal of nitrate in aqueous solution, *Journal of Cleaner Production* 83 (2014) 413–419.
- [21] S. Pu, D. Deng, K. Wang, M. Wang, Y. Zhang, L. Shanguan, W. Chu, Optimizing the removal of nitrate from aqueous solutions via reduced graphite oxide-supported nZVI: synthesis, characterization, kinetics, and reduction mechanism, *Environ Sci Pollut Res Int* 26 (4) (2019) 3932–3945.
- [22] X. Yu, W. Zhang, P. Zhang, Z. Su, Fabrication technologies and sensing applications of graphene-based composite films: Advances and challenges, *Biosens Bioelectron* 89 (2017) 72–84.
- [23] L. Ren, J. Dong, Z. Chi, H. Huang, Reduced graphene oxide-nano zero value iron (rGO-nZVI) micro-electrolysis accelerating Cr(VI) removal in aquifer, *J Environ Sci (China)* 73 (2018) 96–106.
- [24] C. Wang, H. Luo, Z. Zhang, Y. Wu, J. Zhang, S. Chen, Removal of As(III) and As(V) from aqueous solutions using nanoscale zero valent iron-reduced graphite oxide modified composites, *J Hazard Mater* 268 (2014) 124–131.
- [25] Y.-F. Sun, W.-K. Chen, W.-J. Li, T.-J. Jiang, J.-H. Liu, Z.-G. Liu, Selective detection toward Cd²⁺ using Fe₃O₄/RGO nanoparticle modified glassy carbon electrode, *Journal of Electroanalytical Chemistry* 714-715 (2014) 97–102.
- [26] P. Bhunia, G. Kim, C. Baik, H. Lee, A strategically designed porous iron-iron oxide matrix on graphene for heavy metal adsorption, *Chem Commun (Camb)* 48 (79) (2012) 9888.
- [27] Q.i. Zhang, D. Zhao, S. Feng, Y. Wang, J. Jin, A. Alsaedi, T. Hayat, C. Chen, Synthesis of nanoscale zero-valent iron loaded chitosan for synergistically enhanced removal of U(VI) based on adsorption and reduction, *J Colloid Interface Sci* 552 (2019) 735–743.
- [28] Q. Dong, X. Zhuang, Z. Li, B. Li, B. Fang, C. Yang, H. Xie, F. Zhang, X. Feng, Efficient approach to iron/nitrogen co-doped graphene materials as efficient electrochemical catalysts for the oxygen reduction reaction, *Journal of Materials Chemistry A* 3 (15) (2015) 7767–7772.
- [29] R.S. Sahu, D.-L. Li, R.-A. Doong, Unveiling the hydrodechlorination of trichloroethylene by reduced graphene oxide supported bimetallic Fe/Ni nanoparticles, *Chemical Engineering Journal* 334 (2018) 30–40.
- [30] A. Masud, N.G. Chavez Soria, D.S. Aga, N. Aich, Adsorption and advanced oxidation of diverse pharmaceuticals and personal care products (PPCPs) from water using highly efficient rGO-nZVI nanohybrids, *Environmental Science: Water Research & Technology* 6 (8) (2020) 2223–2238.
- [31] J. Wu et al, Removal mechanism of mitoxantrone by a green synthesized hybrid reduced graphene oxide@iron nanoparticles, *Chemosphere* 246 (2020) 125700.
- [32] X. Lv, Y. Zhang, W. Fu, J. Cao, J. Zhang, H. Ma, G. Jiang, Zero-valent iron nanoparticles embedded into reduced graphene oxide-alginate beads for efficient chromium (VI) removal, *J Colloid Interface Sci* 506 (2017) 633–643.
- [33] G. Zhao, J. Li, X. Ren, C. Chen, X. Wang, Few-layered graphene oxide nanosheets as superior sorbents for heavy metal ion pollution management, *Environ Sci Technol* 45 (24) (2011) 10454–10462.
- [34] X. Weng, Z.e. Lin, X. Xiao, C. Li, Z. Chen, One-step biosynthesis of hybrid reduced graphene oxide/iron-based nanoparticles by eucalyptus extract and its removal of dye, *Journal of Cleaner Production* 203 (2018) 22–29.
- [35] R. Liao, Z. Tang, Y. Lei, B. Guo, Polyphenol-Reduced Graphene Oxide: Mechanism and Derivatization, *Journal of Physical Chemistry C* 115 (42) (2011) 20740–20746.
- [36] Y. Zhang et al, Polypyrrole modified Fe(0)-loaded graphene oxide for the enrichment of uranium(vi) from simulated seawater, *Dalton Trans* 47 (37) (2018) 12984–12992.
- [37] A. Goswami, R.G. Kadam, J. Tuček, Z. Sofer, D. Bouša, R.S. Varma, M.B. Gawande, R. Zborůl, Fe(0)-embedded thermally reduced graphene oxide as efficient nanocatalyst for reduction of nitro compounds to amines, *Chemical Engineering Journal* 382 (2020) 122469.
- [38] R. Liu, Y. Xu, B. Chen, Self-assembled nano-FeO(OH)/reduced graphene oxide aerogel as a reusable catalyst for photo-fenton degradation of phenolic organics, *Environ Sci Technol* 52 (12) (2018) 7043–7053.
- [39] S. Yu, X. Wang, Y. Liu, Z. Chen, Y. Wu, Y. Liu, H. Pang, G. Song, J. Chen, X. Wang, Efficient removal of uranium(VI) by layered double hydroxides supported nanoscale zero-valent iron: A combined experimental and spectroscopic studies, *Chemical Engineering Journal* 365 (2019) 51–59.
- [40] C. Xiao et al, Green synthesis of iron nanoparticle by tea extract (polyphenols) and its selective removal of cationic dyes, *J Environ Manage* 275 (2020) 111262.
- [41] H. Tang et al, Nano zero valent iron encapsulated in graphene oxide for reducing uranium, *Chemosphere* 278 (2021) 130229.
- [42] G. Bhargava, I. Gouzman, C.M. Chun, T.A. Ramanarayanan, S.L. Bernasek, Characterization of the “native” surface thin film on pure polycrystalline iron: A high resolution XPS and TEM study, *Applied Surface Science* 253 (9) (2007) 4322–4329.
- [43] Y.-F. Sun, J.-H. Sun, J. Wang, Z.-X. Pi, L.-C. Wang, M. Yang, X.-J. Huang, Sensitive and anti-interference stripping voltammetry analysis of Pb(II) in water using flower-like MoS₂/rGO composite with ultra-thin nanosheets, *Analytica Chimica Acta* 1063 (2019) 64–74.
- [44] M.B. Gumpu, M. Veerapandian, U.M. Krishnan, J.B.B. Rayappan, Simultaneous electrochemical detection of Cd(II), Pb(II), As(III) and Hg(II) ions using ruthenium (II)-textured graphene oxide nanocomposite, *Talanta* 162 (2017) 574–582.
- [45] J. Lu, X.u. Zhang, X. Zhang, N. Liu, H. Li, Z. Yu, X. Yan, Electrochemical sensor for mercuric chloride based on graphene-MnO₂ composite as recognition element, *Electrochimica Acta* 174 (2015) 221–229.
- [46] H. Xing, J. Xu, X. Zhu, X. Duan, L. Lu, W. Wang, Y. Zhang, T. Yang, Highly sensitive simultaneous determination of cadmium (II), lead (II), copper (II), and mercury (II) ions on N-doped graphene modified electrode, *Journal of Electroanalytical Chemistry* 760 (2016) 52–58.
- [47] C.-C. Bi, X.-X. Ke, X. Chen, R. Weerasooriya, Z.-Y. Hong, L.-C. Wang, Y.-C. Wu, Assembling reduced graphene oxide with sulfur/nitrogen- “hooks” for electrochemical determination of Hg(II), *Anal Chim Acta* 1100 (2020) 31–39.
- [48] N.R. Perron, J.L. Brumaghim, A review of the antioxidant mechanisms of polyphenol compounds related to iron binding, *Cell Biochem Biophys* 53 (2) (2009) 75–100.
- [49] C. Kim et al, Mechanisms of electro-assisted persulfate/nano-Fe(0) oxidation process: Roles of redox mediation by dissolved Fe, *J Hazard Mater* 388 (2020) 121739.

- [50] F. Gao, N. Gao, A. Nishitani, H. Tanaka, Rod-like hydroxyapatite and Nafion nanocomposite as an electrochemical matrix for simultaneous and sensitive detection of Hg^{2+} , Cu^{2+} , Pb^{2+} and Cd^{2+} , *Journal of Electroanalytical Chemistry* 775 (2016) 212–218.
- [51] X. Zhu, B. Liu, H. Hou, Z. Huang, K.M. Zeinu, L. Huang, X. Yuan, D. Guo, J. Hu, J. Yang, Alkaline intercalation of Ti_3C_2 MXene for simultaneous electrochemical detection of Cd(II) , Pb(II) , Cu(II) and Hg(II) , *Electrochimica Acta* 248 (2017) 46–57.